Structures of Water Octamers $(H_2O)_8$: Exploration on Ab Initio Potential Energy Surfaces by the Scaled Hypersphere Search Method

Satoshi Maeda and Koichi Ohno*

Department of Chemistry, Graduate School of Science, Tohoku University, Aramaki, Aoba-ku, Sendai 980-8578, Japan

Received: January 24, 2007; In Final Form: March 23, 2007

The potential energy surface (PES) of water octamers has been explored by the scaled hypersphere search method. Among 164 minima on the PES (based on MP2/6-311++G(3df,2p)//B3LYP/6-311+G(d,p) calculations), the cubic structure with D_{2d} symmetry has been confirmed to be the global minimum. In a thermodynamic simulation using these 164 structures, the cubic structure with S_4 symmetry has the highest population at low temperature, though double rings can become dominant as temperature going up, in good accord with a recent Monte Carlo simulation using an empirical potential. A transition temperature from cubic to noncubic has significantly been underestimated when potential energy data of B3LYP/6-311+G(d,p) calculations are employed in the simulation. This serious discrepancy between the MP2 and the B3LYP results suggests an importance of dispersion interactions for discussions on thermodynamics of water octamers.

1. Introduction

The water octamers $(H_2O)_8$ has been studied extensively by both theoretically and experimentally. In an early theoretical study, a cyclic single ring structure was considered by using an analytical potential function fitted to Hartree−Fock water−water interaction energies.[1] A hexagonal ice-like structure was proposed as the most stable form of water octamers in subsequent theoretical studies using the polarization model,[2,3] although a study using empirical model potentials revealed that a cubic structure with D_{2d} symmetry is more stable than the ice-like form,[4] which was confirmed by a subsequent study.[5] Another important cubic structure with S_4 symmetry was discovered in a Monte Carlo simulated annealing study.[6]

The D_{2d} and the S_4 cubes have nearly the same stability, and the global minimum can be altered each other depending on qualities of model potentials.[7−9] In gas-phase experiments of pure[10] and benzene attached[11,12] water octamers, both the D_{2d} and the S_4 cubes have been identified through careful comparisons between experimental and theoretical vibrational spectra of the OH stretch region. It has been shown that these two cubes have the same MP2 complete basis set limit within the error bar of the extrapolation procedure,[13] although the MP2 always computes the D_{2d} energy to be lower when aug-cc-pV*n*Z basis sets are employed. Rearrangement reaction pathways between the D_{2d} and the S_4 cubes have also been investigated.[14,15]

Fourteen cubic structures have been characterized theoretically using empirical model potentials and MP2 calculations.[16−18] Among these 14 cubes, the D_{2d} and the S_4 cubes have special stability in comparison with other higher energy cubes, and there has been no experimental observation of other cubes in gas phase, although a cube with C_i symmetry has been identified in a crystallography.[19]

Another very important subject concerning with water octamers is a transition temperature from the cubic to noncubic structures, and noncubic parts of the potential energy surface (PES) have also been explored.[6,16,20−33] In Monte Carlo or dynamics simulations using various model potentials have estimated the transition temperature will be below the room temperature of 100−230 K.[6,20−26] Some ab initio calculations have also suggested that a single ring structure can become lower in free energy than the cubes at the room temperature.[27−29] A recent Monte Carlo simulation using an empirical potential proposed that double ring structures with nine hydrogen-bonds are the most abundant hydrogen-bond patterns at 200 K.[32] Contrary to these studies, a recent ab initio study suggested that the D_{2d} cube is still the most probable structure at the room-temperature based on the G3 model chemistry and seven cubic and eleven noncubic structures.[33]

In this study, cubic and noncubic parts of the PES of water octamers has been explored by the scaled hypersphere search (SHS) method.[34−36] Although there have been extensive explorations,[16] simulations,[6,20−26,32] and global optimizations[7−9] by using empirical model potentials, the SHS method has directly been applied to an ab initio PES. Although the SHS method has originally been developed for constructing global reaction route maps on PESs of small molecules including entire reaction route networks through equilibrium structures (EQ) and transition state structures (TS), a variation for exploring lower energy EQs only has been introduced to make an application to water octamers. 164 EQs have been obtained on the B3LYP/6-311+G(d,p) PES by the present procedure, and then energy values of each EQs have been refined at the MP2/6-311++G(3df,2p) level. The database including coordinates, relative energies, and harmonic frequencies for these 164 EQs is available in Supporting Information. Thermodynamic simulations have been performed by using the database, and finite temperature behaviors of water octamers based on the present database have been compared with previous Monte Carlo simulations using empirical potentials.[23,26,32]

2. The Scaled Hypersphere Search Method

The scaled hypersphere search (SHS) method is an uphill walking technique on a potential energy surface (PES) starting

* Corresponding author. Tel: +81-22-795-6576. Fax: +81-22-795-6580. E-mail: ohnok@mail.tains.tohoku.ac.jp.

10.1021/jp070606a CCC: $37.00
Published on Web 04/27/2007

from an equilibrium structure (EQ) toward transition state structures (TS) or dissociation channels (DC).[34−36] The SHS method can follow approximate reaction pathways from an EQ based on a simple principle of chemical reactions "reaction pathways can be detected and then followed starting from an equilibrium structure by noting anharmonic downward distortions as symptoms of chemical reactions". This principle is based on a consideration on characteristic features of PESs. Typical reaction paths always change their curvatures from a concave to a convex on going to a TS or a DC. This indicates that slopes should always decline their inclinations anharmonically because of the energy lowering interactions leading to a TS or a DC. Thus, one may expect that reaction pathways can be found as anharmonic downward distortions (ADD) around an EQ on a quantum chemical PES.

Directions containing the maximal ADD can be detected as energy minima on a scaled hypersphere surface centered at the starting EQ, when one employs the scaled normal coordinates $q_i = \lambda_i^{1/2} Q_i$ based on normal coordinates Q_i and corresponding Eigenvalues λ_i obtained by the normal-mode analysis at the EQ. The ADD following by the SHS method can be used for finding many reaction pathways around an EQ, and a one-after-another algorithm has been established for global reaction route mapping (GRRM) on a quantum chemical PES by combining downhill walking by the intrinsic reaction coordinate[37] (IRC) following techniques[38,39] with uphill walking by the SHS method.[34−36]

In GRRM by the one-after-another algorithm, all possible reaction pathways leading ADDs are followed starting from all obtained EQs in the process to disclose whole IRC network via EQs and TSs. Although this has successfully been applied to small systems with 5−7 atoms, its application to larger systems including more than 20 atoms may not be straightforward, since numbers of EQs of larger systems should be so many that applications of the SHS procedure to all obtained EQs can be impossible. In this study, some simplifications, including a parallel tempering Monte Carlo simulation[40,41] like treatment, have been introduced to explore lower free energy structures of water octamers at various temperatures (see Appendix for details).

3. Results

The SHS method was applied to a PES of water octamers based on the RHF/6-31G calculations. In total, 181 EQs were obtained by the application. These 181 structures were confirmed to be minima by normal-mode analyses at each structure; in 119 of 181 EQs were found in a search starting from the first initial structure among 24 initial structures, and subsequent searches starting from other initial structures were finished very quickly with rediscovering old EQs to which the SHS procedure has already been applied in previous searches. Moreover, all of important EQs (cubes, double rings, and a single ring) discussed below were included in these 119 EQs. It follows that the present parametrizations for *n*, *m*, and *l* (see Appendix) can be sufficient to explore lower energy EQs of water octamers. In total, 212 444 times force calculations and 6427 times Hessian calculations were required to complete the procedure. These numbers are comparable with those required for GRRMs of 5−7 atom systems, and so the calculation was completed within 1 month by using one CPU (Itanium 2, 1.6 GHz).

EQs obtained by the SHS method were re-optimized on a PES based on the B3LYP/6-311+G(d,p) calculations using these 181 EQs as initial guesses for geometry optimizations. 164 EQs were obtained as minima (confirmed by normal-mode analyses) on the B3LYP/6-311+G(d,p) surface, although 17 initial guesses were collapsed into lower energy EQs during geometry optimizations. Then, single point energies at these 164 EQs were refined by the MP2/6-311++G(3df,2p) calculation. In this series of calculations, energy values, gradient vectors, and Hessian matrices at each geometrical arrangement were obtained from the GAUSSIAN03 programs.[42] Other parts such as the SHS procedure, geometry optimizations by the rational function optimization (RFO) method,[43] and normal-mode analyses were made by the GRRM1.0 programs written by the authors[35,36] based on potential energy data from the GAUSSIAN03. Cartesian coordinates and relative energies of these 164 EQs are given in Supporting Information.

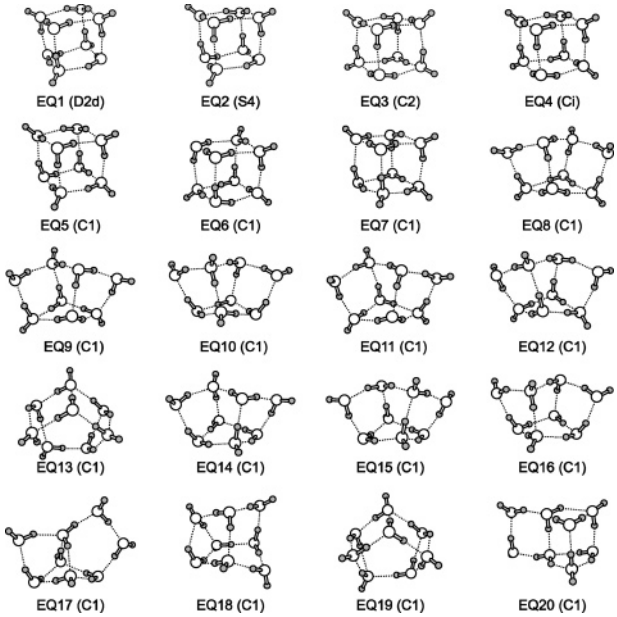

Figure 1. The 20 lowest potential energy structures among the 164 EQs.

Figure 1 shows the 20 lowest potential energy structures among the 164 EQs. Their relative energy values (potential energies ΔE, internal energies ΔU, and free energies ΔG at 400 K) are listed in Table 1, where internal energies and free energies were estimated using structures and harmonic frequencies of the B3LYP/6-311+G(d,p) calculations. As has been reported in previously, the cubic structure with D_{2d} symmetry (EQ1) is the lowest-energy structure among the present 164 EQs. Although 14 cubic structures are known for water octamer,[16−18] six of those have higher energy than 25 kJ/mol relative to the lowest-energy cubic structure with D_{2d} symmetry,[18] and these higher energy cubes have not been found in the present application of the SHS method because of the simplifications to search for lower energy structures only. Among eight lower energy cubic structures, a structure with C_s symmetry has not been included in the present results, because its relative energy to the D_{2d} structure is also higher than 25 kJ/mol on the RHF/6-31G surface. This is a problem to make an application of the SHS method to the lower quality RHF/6-31G surface, although effects of an inclusion of the C_s cube have been very small on the following thermodynamic simulations. There have been many distorted cubes such as EQ8 with eleven hydrogen bonds at 22−26 kJ/mol above the D_{2d} cube, some of them can be lower in free energy than some of cubes at higher temperatures by the entropy effect due to the smaller number of hydrogen bonds.

Figure 2 shows the 20 lowest free energy structures (at 400 K) among the 164 EQs. Their relative energy values (potential energies ΔE, internal energies ΔU, and free energies ΔG at 400 K) are listed in Table 1, where internal energies and

TABLE 1: Relative Energies (in kJ/mol) for Equilibrium Structures (EQ) in Figures 1 and 2[a]

	MP2/6-311++G(3df,2p)[b]			B3LYP/6-311+G(d, p)		
	ΔE	ΔU[c]	ΔG[c]	ΔE	ΔU[c]	ΔG[c]
EQ1	0.0	0.1	5.3	0.0	0.3	21.5
EQ2	0.3	0.0	2.4	0.1	0.0	18.5
EQ3	12.7	10.1	10.0	13.1	10.6	26.6
EQ4	13.1	11.4	9.3	13.0	11.4	25.4
EQ5	17.3	14.3	10.8	17.7	14.8	27.5
EQ6	17.6	14.7	11.4	18.3	15.5	28.2
EQ7	18.0	15.4	11.9	18.3	15.8	28.4
EQ8	22.5	17.4	6.7	20.1	15.1	20.5
EQ9	23.5	18.0	7.2	20.3	14.9	20.2
EQ10	23.9	18.6	8.6	21.0	15.8	21.9
EQ11	24.2	18.8	7.8	21.8	16.6	21.6
EQ12	25.1	19.9	9.5	22.1	17.0	22.7
EQ13	25.7	21.0	12.1	22.4	17.9	25.0
EQ14	26.1	20.6	9.9	23.7	18.4	23.8
EQ15	26.1	20.6	10.3	22.7	17.3	23.1
EQ16	26.4	21.0	10.3	25.0	19.8	25.2
EQ17	28.3	21.7	8.1	25.7	19.3	21.8
EQ18	28.3	21.7	9.1	23.3	16.7	20.2
EQ19	28.6	23.2	13.0	26.7	21.4	27.3
EQ20	28.8	23.2	8.8	26.9	21.5	23.2
EQ21	44.4	32.7	0.0	32.3	20.7	4.1
EQ22	47.4	34.8	0.4	33.0	20.6	2.2
EQ23	53.3	39.2	0.4	40.9	27.0	4.3
EQ24	43.7	32.2	0.5	31.5	20.1	4.5
EQ25	44.4	32.8	0.9	32.3	20.8	5.0
EQ26	44.5	32.9	1.0	32.4	20.9	5.0
EQ27	45.4	33.3	1.0	31.3	19.3	3.1
EQ28	50.5	37.1	1.2	36.7	23.3	3.6
EQ29	47.6	34.7	1.9	33.5	20.8	4.0
EQ30	31.6	22.8	2.1	24.5	15.9	11.2
EQ31	45.6	33.7	2.2	31.4	19.7	4.2
EQ32	50.0	36.9	2.5	35.6	22.6	4.3
EQ33	45.6	33.8	2.8	35.6	23.9	8.9
EQ34	48.0	35.5	3.0	33.2	20.8	4.4
EQ35	40.1	29.5	3.1	31.1	20.6	10.3
EQ36	43.2	32.3	3.1	32.9	22.1	9.0
EQ37	48.1	35.5	3.3	33.0	20.5	4.4
EQ38	51.5	38.6	3.6	37.7	24.9	6.0
EQ39	64.5	46.5	4.3	43.9	26.0	0.0

[a] Relative potential energies ΔE, relative internal energies ΔU, and relative free energies ΔG (at 400 K) are shown with respect to the lowest-energy structure. [b] At optimized structures on the B3LYP/6-311+G(d,p) surface. [c] Estimated using harmonic frequencies by B3LYP/6-311+G(d,p) calculations.

free energies were estimated using structures and harmonic frequencies of the B3LYP/6-311+G(d,p) calculations. Most of low free energy EQs in Figure 2 are double ring structures except for EQ2, 30, 33, 35, and 36, in good accord with a recent Monte Carlo simulation by Miyake and Aida.[32] In the following discussions, double rings (DR) composed of four-membered and five-membered rings, two five-membered rings, four-membered and six-membered rings, and three-membered and seven-membered rings are denoted as DR45, DR55, DR46, and DR37, respectively. DR37s have also been obtained, although they are not included in Figure 2. In total, there are four DR45s, four DR55s, seven DR46s and two DR37s in the 164 EQs. The single ring structure with S_8 symmetry is also stable at high temperature as suggested in previous papers.[27−29] Although these double and single rings are much higher in potential energy than the D_{2d} cube (the S_8 single ring is the highest potential energy structure among the 164 EQs), many such ring structures could safely be detected in this study owing to the parallel tempering simulation[40,41] like treatment to search for lower free energy structures at eleven different temperatures (see Appendix). These rings can be very important at higher temperatures,[27−29,32] since they have extremely low-frequency vibrational normal modes corresponding to their bending and twisting motions. These low-frequency motions enlarge their vibrational entropy, and consequently, they have very low free energy at higher temperatures.

4. Discussion

A. Thermodynamic Simulation. To compare the present results with previous studies in more detail, thermodynamic simulations have been performed based on the superposition approach[44,45] using the present 164 EQs. The canonical probability of finding a system in a region "*A*" is[45]

$$P_{\mathrm{A}} = \frac{\sum_{i\in \mathrm{A}} Z_i(T)}{\sum_i Z_i(T)} \tag{1}$$

where Z_i is the partition function of *i*-th minimum. Z_i can be obtained based on the harmonic approximation around each minimum as[45]

$$Z_i(T) = \frac{2N!\,\exp(-\beta E_i)}{m_i \prod_j^{3N-6} (\beta h \nu_{ij})} \tag{2}$$

where m_i is the order of point group of *i*-th minimum, E_i is the potential energy of *i*-th minimum, ν_{ij} is *j*-th harmonic frequency

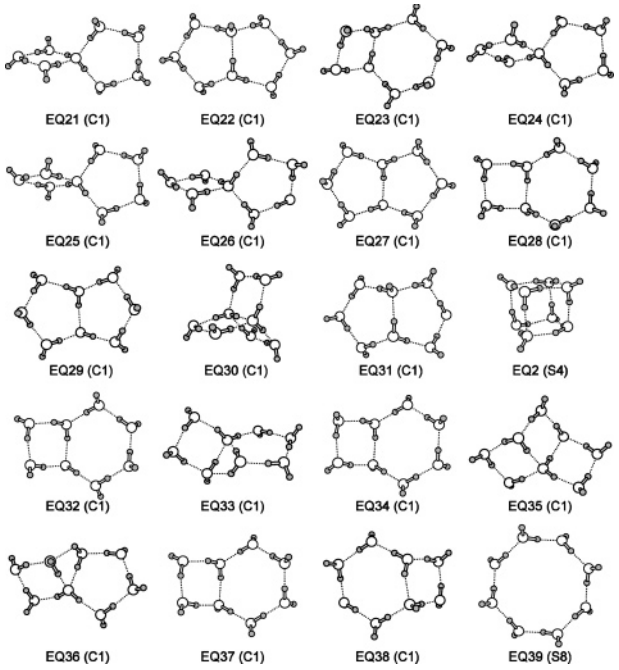

Figure 2. The 20 lowest free energy structures at 400 K among the 164 EQs.

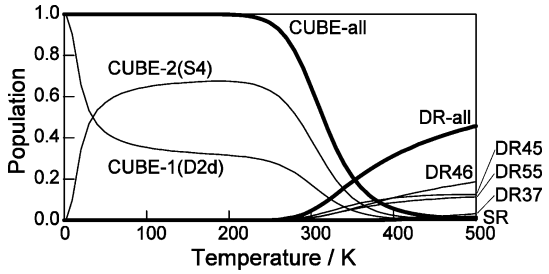

Figure 3. Temperature dependences of populations of cubic structures (CUBE-all), double ring structures (DR-all), and the single ring (SR) (thick lines) and temperature dependences of populations of the D_{2d} cube, the S_4 cube, DR45s, DR55s, DR46s, and DR37s (thin lines), based on the MP2/6-311++G(3df,2p) energy values.

of i-th minimum, N is the number of atoms, and $\beta = 1/kT$. In this study, cubes, double rings, and the single ring have been considered as regions "A" in eq 1. Contributions from the D_{2d} cube, the S_4 cube, DR45s, DR55s, DR46s, and DR37s have further been decomposed into individual components for more detailed discussions. The summation in the denominator in eq 1 has been taken over the all of 164 EQs.

Temperature dependences of populations of cubic structures (CUBE-all), double ring structures (DR-all), and the single ring (SR) are shown in Figure 3 with thick lines. Thin lines show temperature dependences of populations of the D_{2d} cube, the S_4 cube, DR45s, DR55s, DR46s, and DR37s, respectively. Figure 3 is based on MP2 energies and B3LYP harmonic frequencies for E_i and ν_{ij} in eq 2, respectively.

As can be seen in Figure 3, contributions from the D_{2d} cube and the S_4 cube amount to almost 100% at low temperatures, agrees well with the observations of these two cubes in gas-phase[10−12] as well as previous simulations.[6,20−26] As suggested previously,[6] the S_4 cube can be more probable at medium temperatures than the D_{2d} cube because of lower point group order (m_i) in the denominator of eq 2. Contributions from other cubes have been very small no more than 9% with a maximum around 300 K, although this 9% is slightly smaller than in the previous simulation of 12%[26] probably because of lack of C_s and higher energy cubes in the present simulation. Although the Boltzmann distribution for cubic structures at 298.15 K was estimated to be about 90% in the recent G3 study based on 18 EQs and the harmonic approximation around each EQ,[33] the present estimate based on eqs 1 and 2 and the 164 EQs is about 65%. This discrepancy can be explained from the difference in the numbers of EQs considered in each simulation, since 125 EQs with populations of only 0.2% on average can reduce the cube's population from 90% to 65%. The population of cubic structures becomes smaller than 50% around 310 K. It follows that the present estimate of the transition temperature T_t of water octamers can be about 310 K, although there may be some ambiguities on the T_t as discussed below.

At first, one needs to consider about the accuracy of the quantum chemical calculations. It has been shown by Xantheas and Aprà that the discrepancy between the binding energy values of the D_{2d} cube computed by MP2 and CCSD(T) is smaller than 0.04 kcal/mol (0.17 kJ/mol),[13] and so the effects of higher electron correlation may not change the T_t value significantly. While, corrections on the basis set superposition error (BSSE) and the error of B3LYP harmonic frequencies can shift the T_t 10−20 K to lower and ca. 55 K to higher, respectively, as estimated in Sections 4D and 4E. Another important error that should be taken into account is caused by the harmonic approximation assumed in eq 2. Anharmonic corrections can be crucial in cluster systems, and Doye and Wales demonstrated that $T_t^{anharmonic}/T_t^{harmonic}$ are 0.82 and 0.87 for Lennard−Jones clusters of LJ_{13} and LJ_{55}, respectively.[44] Since Lennard-Jones (rare-gas) clusters are more floppy than hydrogen bonding ones, $T_t^{anharmonic}/T_t^{harmonic}$ for water octamers may be larger than these values. Finally, present estimate of the T_t value is 280−320 K, after considerations on the BSSE correction of 10−20 K, the correction concerning with the quality of B3LYP harmonic frequencies of ca. 55 K, and the anharmonic correction of $0.9 > T_t^{anharmonic}/T_t^{harmonic} > 0.82$.

There have been many Monte Carlo and dynamics simulations using empirical model potentials.[6,20−26] According to extensive simulations by Pedulla and Jordan using seven different empirical potentials,[23] T_t can vary between 112 and 228 K depending on qualities of employed model potentials. For an example, the TIP3P and the TIP4P models[46] gave about 100 K different values of $T_t = 112$ K[23] and $T_t = 212$ K,[26] respectively. On the other hand, the lower bound of the present estimate of 280 K is higher than all of these values. Although the MP2 surface employed in this study may be the more reliable than model potentials, there are still some ambiguities in the present calculations as mentioned above and discussed in detail in the following Sections 4D and 4E. The more reliable estimation on the T_t value may be achieved if all of present 164 EQs are treated by a high-level ab initio calculation with a very large basis set.

Relations among the present $T_t \approx 310$ K without any corrections, $T_t \approx 210$ K by TIP4P,[26] and $T_t \approx 110$ K by TIP3P[23] indicate that Figure 2 for 400 K in this study can be compared with the 200 K results of the recent Monte Carlo simulation using the TIP3P potential by Miyake and Aida,[32] and Figure 2 may supports their finding that double ring structures with nine hydrogen bonds can be the most abundant hydrogen-bond patterns at the temperature. Finally, we may conclude that the present database including 164 B3LYP structures and their MP2 energies can qualitatively be consistent with previous Monte Carlo simulations using empirical model potentials[23,26,32] over a fairly wide temperature range.

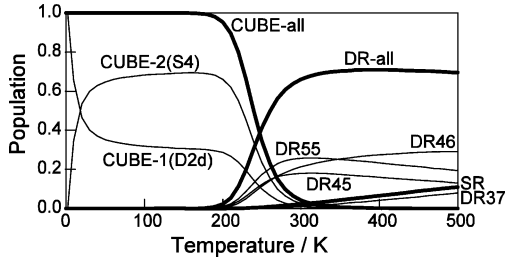

Figure 4. Temperature dependences of populations of cubic structures (CUBE-all), double ring structures (DR-all), and the single ring (SR) (thick lines) and temperature dependences of populations of the D_{2d} cube, the S_4 cube, DR45s, DR55s, DR46s, and DR37s (thin lines), based on the B3LYP/6-311+G(d,p) energy values.

B. MP2 Energy and B3LYP Energy. As can be seen in Table 1, energetics based on the MP2 method and the B3LYP method is significantly different especially for EQ21−EQ39 in Figure 2. The magnitudes of these discrepancies seem to be depending on numbers of hydrogen bonds. Differences between MP2 energies and B3LYP energies are smaller than 1 kJ/mol for cubic structures of EQ1−7 with twelve hydrogen bonds, larger than 2 kJ/mol for distorted cubes such as EQ8 with eleven hydrogen bonds, 5−10 kJ/mol for triple rings such as EQ30 with ten hydrogen bonds, larger than 10 kJ/mol for double rings with nine hydrogen bonds, the largest of 21 kJ/mol for the single ring with eight hydrogen bonds.

This propensity can be explained based on the long-range dispersion interactions that cannot be described by the B3LYP functional. Dispersion energy can be expressed by r^{-6} terms centered at each atom in conventional force field methods.[47] Since dispersion energy can be explained by instantaneously induced dipole−dipole interactions due to dynamical electron correlations, their magnitudes can depend on numbers of electrons. In the case of water clusters, dispersion energies are mainly governed by oxygen−oxygen distance r_{O-O},[46] since most of electrons are distributed around oxygen atoms. Thus, dispersion interactions can be the more important for the more compact structures with many smaller O−O distances, and consequently, the energy splitting between cubes and rings become larger when dispersion interactions are taken into account by the MP2 method.

This discrepancy between MP2 energies and B3LYP energies can be visualized when the thermodynamic simulation is performed. Figure 4 shows the results of the simulation using the B3LYP/6-311+G(d,p) energies, where all notations are the same as Figure 3. The transition temperature significantly shifts to lower in Figure 4 in comparison with Figure 3. Although $T_t \approx 240$ K estimated from Figure 4 shows better fit to the TIP4P simulations,[26] this should be an accident caused by cancellations between lack of dispersion energy and BSSE and anharmonic corrections. Some previous thermodynamics studies based on HF or DFT potential energy data[28,29] may also suffer from this drawback to result in indicating an importance of ring structures at room-temperature based on the harmonic approximation. Figure 4 overestimates populations of double rings in comparison with Figure 3, while populations in Figure 3 for DR45, DR55, and DR46 are around 10% at 400 K in good accord with the recent Monte Carlo simulation.[32] Oppositely, the B3LYP result underestimates importance of triple rings such as EQ30 as can be seen in Table 1 of their free energies. Therefore, discussions or simulations using B3LYP energies can be dangerous for water clusters when structures containing different numbers of hydrogen bonds are compared.

TABLE 2: MP2/6-311++G(3df,2p) Energies Calculated at Different Geometries Based on Different Methods (B3LYP or MP2) and Basis Sets[a]

method	basis	EQ1	EQ2	EQ27	EQ39
B3LYP	6-31G	61.86	63.28	68.57	64.59
	6-31G(d)	9.69	10.11	b	15.19
	6-31+G	43.05	43.96	54.90	52.38
	6-31+G(d)	3.33	3.51	4.10	4.81
	6-31+G(d,p)	1.38	1.60	2.23	2.72
	6-311+G(d)	1.69	2.12	2.98	3.36
	6-311+G(d,p)	−0.61	−0.39	0.25	0.54
	6-311++G(d,p)	−0.61	−0.38	0.20	0.55
MP2	6-31G	28.03	29.23	33.26	29.50
	6-31G(d)	4.43	4.61	b	8.39
	6-31+G	34.02	34.86	38.38	33.00
	6-31+G(d)	4.43	4.60	5.57	6.48
	6-31+G(d,p)	0.12	0.29	0.33	0.71
	6-311+G(d)	2.53	2.85	4.62	3.50
	6-311+G(d,p)	0.04	0.07	0.06	−0.13

[a] Energies (in kJ/mol) are relative to the single-point energies at the MP2/6-311++G(d,p) geometry. [b] Geometry optimization using the double ring structure as an initial guess collapsed into a three-dimensional structure with lower potential energy.

C. Reliability of B3LYP Geometry. Although energy values are very different between MP2 and B3LYP when numbers of hydrogen bonds are different, geometries have not been very much sensitive to the levels of calculations. This may be because dispersion interactions among water molecules are almost isotropic as assumed in many model potentials such as TIP4P, where r^{-6} terms are placed at each oxygen atom without Legendre expansions.[46] Table 2 shows MP2/6-311++G(3df,-2p) energies at different geometries based on different combinations of methods (MP2 or B3LYP) and basis sets, where energy values are relative to the MP2/6-311++G(3df,2p) potential energies at the MP2/6-311++G(d,p) geometry. Two lowest-energy cubes (EQ1 and EQ2), the lowest-energy double ring composed of two five-membered rings (EQ27), and the single ring (EQ39) were chosen for the following comparisons.

The 6-31G and 6-31+G basis sets cannot be acceptable in both MP2 and B3LYP calculations even about relative energy values. Additions of polarization functions to oxygen atoms can significantly improve the absolute deviations, although the relative energy of EQ39 with respect to EQ1 is overestimated more than 5 kJ/mol. Moreover, an important double ring structure of EQ27 is lacking on both MP2/6-31G(d) and B3LYP/6-31G(d) surfaces. At least the 6-31+G(d) basis set is required for both MP2 and B3LYP calculations to obtain reliable geometries as suggested in studies on $H^+(H_2O)_n$ clusters[48] and $NH_4^+(H_2O)_n$ clusters.[49] According to Table 2, the B3LYP/6-311+G(d,p) geometries employed in this study may yield errors of about 1 kJ/mol with respect to the MP2/6-311++G(d,p) geometries, which is much smaller than errors of dispersion energies described above as well as BSSEs discussed below.

D. Basis Set Superposition Errors. The MP2/6-311++G-(3df,2p) energies should be compared with the MP2 complete basis set (CBS) limit estimated by Xantheas and Aprà[13] to evaluate basis set superposition errors (BSSE) in the present result. The total binding energy E_B without BSSE correction can be calculated as

$$E_B = -(E_{cluster} - 8E^{Monomer\_basis}_{Monomer\_geometry}) \quad (3)$$

where, $E_{cluster}$ is the energy of a water octamer, $E^{Monomer\_basis}_{Monomer\_geometry}$ is the energy of an isolated water molecule. The total binding

TABLE 3: Estimations of the Basis Set Superposition Error (BSSE) of MP2/6-311++G(3df,2p) Calculations[a]

	EQ1	EQ2	EQ27	EQ39
E_B	322.8	322.5	277.4	258.3
$E_B^{(FCP)}$	278.2	277.9	241.1	225.9
$E_B - E_B^{(FCP)}$	44.6	44.7	36.2	32.4
CBS[b]	304.2 ± 1.7	304.2 ± 1.7		
E_B[c]	304.2	303.9	262.2	244.8

[a] Binding energies (in kJ/mol) with ($E_B^{(FCP)}$) and without (E_B) BSSE corrections (by the full counterpoise (FCP) method) are calculated by using eqs 4 and 3, respectively. [b] Complete basis set limit values taken from ref 13. [c] Improved binding energies so that E'_B for EQ1 reproduces the CBS value in ref 13, by using a simple equation, $0.583E_B + 0.417E_B^{(FCP)}$.

energy with the BSSE correction by the full counterpoise (FCP) method[50] $E_B^{(FCP)}$ can be calculated as[13]

$$E_B^{(FCP)} = -(E_{cluster} - \sum_{i=1}^{8} E^{Cluster\_basis}_{Cluster\_geometry}(i) + \sum_{i=1}^{8} E^{Monomer\_basis}_{Cluster\_geometry}(i) - 8E^{Monomer\_basis}_{Monomer\_geometry}) \quad (4)$$

where, $E^{Cluster\_basis}_{Cluster\_geometry}(i)$ is the energy of the *i*-th water molecule in a cluster with the cluster basis, $E^{Monomer\_basis}_{Cluster\_geometry}(i)$ is the energy of the *i*-th water molecule in a cluster with the monomer basis.

Table 3 shows E_B and $E_B^{(FCP)}$ for the same set of EQs in Table 2 of EQ1, EQ2, EQ27, and EQ39. The MP2/6-311++G(3df,2p) method overestimates the E_B about 18−19 kJ/mol at geometries of EQ1 and EQ2 in comparison with the MP2/CBS limit[13] also listed in Table 3. Oppositely, $E_B^{(FCP)}$ underestimates the MP2/CBS limit of EQ1 and EQ2. Since magnitudes of BSSE corrections are not equivalent for different structures but depend on overlap between basis functions on different water molecules, $E_B - E_B^{(FCP)}$ listed in Table 3 are larger for compact cubic structures than rings, where $E_B - E_B^{(FCP)}$ for two cubes are comparable, smaller in a double ring of EQ27, and the smallest in the single ring of EQ39. It follows that BSSE corrections can shift the transition temperature to lower.

Typically, E_B decreases and $E_B^{(FCP)}$ increases as sizes of basis sets become larger, and so it may be reasonable to make a very crude estimation of the CBS value using E_B and $E_B^{(FCP)}$. In this study, E_B values in Table 3 were improved so that E'_B for EQ1 reproduces the MP2/CBS value by Xantheas and Aprà[13] by using a simple equation, $E'_B = 0.583E_B + 0.417E_B^{(FCP)}$. This crude correction shifts relative energies of EQ27 and EQ39 to lower 3.4 kJ/mol and 5.1 kJ/mol, respectively, relative to EQ1.

To know effects of these BSSE corrections, a thermodynamic simulation has been made using a data where energies of the single ring and all double rings are artificially shifted to lower 5.1 kJ/mol and 3.4 kJ/mol, respectively. In this simulation, the transition temperature T_t has shifted about 10 K to lower in comparison with Figure 3. Many other EQs with ten or eleven hydrogen bonds such as triple rings and distorted cubes should become slightly more stable (ca. 1−3 kJ/mol) relative to the D_{2d} cube. Therefore, the BSSE corrections for the 6-311++G(3df,2p) basis set can shift the T_t more than 10 kJ/mol to lower.

E. MP2 Frequencies and B3LYP Frequencies. The population by eqs 1 and 2 depends on a ratio of product of vibrational frequencies, $\prod_j^{66} h\nu_{ij}$, of each structure, and so it is important to check a quality of harmonic frequencies. Table 4 compares

TABLE 4: Comparisons between Products of Harmonic Frequencies, $\prod_j^{66} h\nu_{ij}$, in the Denominator of Eq 2 (in cm^{-66}) Based on the MP2/6-311+G(d,p) Method and the B3LYP/6-311+G(d,p) Method

	EQ1	EQ2	EQ27	EQ39
MP2	1.79×10^{188}	1.51×10^{188}	4.48×10^{183}	1.23×10^{181}
B3LYP	1.22×10^{189}	9.78×10^{188}	5.14×10^{183}	1.36×10^{181}
ratio[a]	0.15	0.15	0.87	0.91

[a] $\prod_j^{66} h\nu_{ij}^{MP2} / \prod_j^{66} h\nu_{ij}^{B3LYP}$.

$\prod_j^{66} h\nu_{ij}$ values based on the MP2 method and the B3LYP method for the same set of EQs in Table 2 of EQ1, EQ2, EQ27, and EQ39. As can be seen in Table 4, $\prod_j^{66} h\nu_{ij}$ values for all EQs in the table are overestimated by the B3LYP method in comparison with MP2 values. This is not expected from the results of rigid molecules, where the MP2 almost always gives higher frequency values and requires the smaller scaling factor of ∼0.94 in comparison with the factor for B3LYP frequencies of ∼0.98.

As expected, the MP2 method overestimated frequencies of intramolecular motions also in the present calculations. While, MP2 frequencies for intermolecular motions were mostly smaller than corresponding B3LYP frequencies. There are the more intermolecular vibrational modes in the case of water octamers, and consequently, $\prod_j^{66} h\nu_{ij}$ values by the MP2 method become smaller than those by the B3LYP method. Although the ratios, $\prod_j^{66} h\nu_{ij}^{MP2} / \prod_j^{66} h\nu_{ij}^{B3LYP}$, in Table 4 increase in the order of EQ1,EQ2 < EQ27 < EQ39 depending on numbers of hydrogen bonds, this can also be consistent with the lack of the r^{-6} long-range interaction in B3LYP calculations. Since the r^{-6} term is fairly defuse in comparison with other interaction terms such as the $e^{-\alpha r}$ term for orbital interactions, it moves the well position to a longer hydrogen-bond distance and can modify the well to be flatter. Therefore, an inclusion of the r^{-6} interactions by the MP2 method can lower the intermolecular vibrational frequencies, especially in structures with many smaller O−O distances.

Table 4 indicates that the population of cubes will be underestimated about six times in coexisting regions of cubes and double rings, when B3LYP frequencies are employed. It follows that a temperature where the population of cubes becomes ca. 0.14 can be a crude estimation of the T_t based on the MP2 frequencies. Since the population of cubes becomes 0.14 around 365 K in the thermodynamic simulation using B3LYP frequencies, the use of the MP2 frequencies can shift the T_t about 55 K to higher.

5. Conclusions

An ab initio potential energy surface (PES) of water octamers has been explored by using the scaled hypersphere search (SHS) method.[34−36] 181 equilibrium structures (EQ) have been obtained on the RHF/6-31G surface. Then, 164 EQs have been confirmed as energy minima on the B3LYP/6-311+G(d,p) surface by subsequent geometry optimizations using the RFO method[43] and the 181 EQs on the crude surface as initial guesses. Single-point energy values for each EQ have been refined at the MP2/6-311++G(3df,2p) level. Cartesian coordinates and relative energies for the 164 EQs are available in the Supporting Information.

Among fourteen known cubic structures,[16−18] seven low-lying cubes have been found in the present application because of simplifications of the SHS procedure to explore lower free energy EQs only at eleven different temperatures (see Appendix for details). This parallel tempering simulation[40,41] like treatment

allowed to explore higher potential energy isomers with low free energies such as double ring structures that can be very important at higher temperature by vibrational entropy effects.

A thermodynamic simulation based on the 164 EQs and the superposition approach[44,45] with the harmonic approximation has supported the finding in the recent Monte Carlo simulation that double ring structures with nine hydrogen bonds can be the most abundant hydrogen-bond patterns at higher temperature.[32] Thermodynamics at low temperatures have been consistent with experimental observations[10−12] as well as previous simulation studies,[6,20−26] where the D_{2d} and the S_4 cubes are dominant. The present estimate of the transition temperature from cubic to noncubic structures are around room temperature of 280−320 K after considerations on the anharmonic correction,[44] the basis set superposition error (BSSE),[13] and the quality of harmonic frequencies. Although the lower bound of the present transition temperature of 280 K is higher than the values by the Monte Carlo simulations using various model potentials,[23] qualitative feature of the present thermodynamic simulation results were consistent with previous Monte Carlo simulations using empirical model potentials[23,26,32] over a fairly wide temperature range. Relative energy values based on the MP2 calculations have been very different from those of the B3LYP calculations when structures with different numbers of hydrogen bonds are compared, and the transition temperature has been underestimated when the B3LYP energy data are employed in the simulation, which suggests an importance of dispersion interactions for discussions on thermodynamics of water octamers.

Finally, we conclude that the SHS method with the present modification can be a powerful tool to explore many EQs on ab initio PESs of molecular clusters. Although an extensive Monte Carlo or dynamics simulation based on a reliable PES has been required to describe finite temperature behaviors of molecular clusters, their applications may be limited to empirical or semiempirical model potentials when single laboratory size computation resources are considered. The water clusters is one of the best established systems where reliable model potentials are available, while further applications of the present approach to other molecular clusters, binary mixtures, or charged clusters may be straightforward, for studies on thermodynamics at low temperature and for (at least qualitative) discussions about finite temperature behaviors, even when an accurate model potential is not available, since our method can directly be applied to ab initio PESs.

6. Appendix

Some simplifications of the scaled hypersphere search (SHS) method[34−36] have been introduced in this study to explore lower energy parts only of ab initio potential energy surfaces (PES) of molecular clusters, and are descried below.

The SHS procedure is not applied to all equilibrium structures (EQ) in the current EQ list but applied to only n lowest free energy EQs. Free energy for each EQ is estimated by using the harmonic vibrational frequencies of each EQ, and eleven different temperatures, 0, $T_{max}/10$, $2T_{max}/10$, ..., T_{max}, are considered in one application. This treatment is introduced to sufficiently explore both lower and higher potential energy regions with low free energies, and this might be related to the parallel tempering Monte Carlo simulation method[40,41] for sampling the wider area on a PES overcoming large potential barriers. At first, energy at 0 K is considered until applications of the SHS procedure to n lowest-energy EQs are completed. Then, free energies at $T_{max}/10$ are considered. If n lowest free energy EQs at a lower temperature is updated during the search at a higher temperature, temperature is decreased to the lower temperature. The SHS procedure is repeated until applications to n lowest free energy EQs at T_{max} are completed. In the present application, $n = 24$ (the number of atoms in water octamers) and $T_{max} = 298.15$ K were employed.

The above treatment is repeated by using m random initial structures as starting points. A random structure is obtained by distributing H_2O with random orientation in a certain ellipsoid where lengths of three axes are also randomized to consider not only three-dimensional structures but also quasi-planar and quasi-linear structures. A problem that H_2 and HOOH appear in the first geometry optimization has been encountered sometimes, and so an initial structure is discarded when H_2 exists during the first geometry optimization. In the present application, $m = 24$ (the number of atoms in water octamers) was used.

An application of the SHS procedure to an EQ has also been simplified. In general applications for global reaction route mapping (GRRM), all possible anharmonic downward distortions (ADD) obtained by the iterative optimization elimination (IOE) technique are followed.[35] Here, one may consider about the Bell-Evans-Polanyi (BEP) principle that a location of a transition state structure (TS) leading to a lower energy EQ is much closer to the current EQ than that connected with higher energy EQs.[51,52] The BEP principle has also successfully been used in the minima hopping technique for global optimization.[53] Based on the BEP principle, a criterion can be employed to reduce a number of ADDs to be followed that l largest magnitude ADDs are selected as important reaction pathways leading to lower energy EQs, since larger stabilization interactions creating the lower energy EQ should have the larger influence around the current EQ to deform its harmonic potential downward. The IOE is a technique to search for ADDs (i.e., energy minima on a scaled hypersphere surface) using an energy minimization and a surface biasing approach, in which an ADD can be eliminated by a cosine cubic function after the ADD was detected by an energy minimization.[35] A search for l largest ADDs by the IOE is very much easier in comparison with the case on a whole PES because of the following reasons; (1) an initial search for ADDs can be made on a very small hypersphere with its radius of ca. 0.03−0.1 Å, (2) all coordinates have cyclic boundary condition in which all points on a scaled hyper-hemi-sphere can be reached with a minimization step length of $\pi/2$, which corresponds to a step length of only 0.08 Å when a radius of a hypersphere is 0.05 Å. In this study, the plus and the minus directions of the softest normal mode are chosen as starting points of energy minimizations on a scaled hypersphere. At first, one minimum is obtained by an energy minimization using the rational function optimization (RFO) method,[43] and then the minimum is eliminated by a cosine cubic shape function. On a modified surface without the first minimum, one can obtain another minimum even when an energy minimization is started from the same point. This optimization-elimination procedure is repeated to search for many ADDs. Typically, $2l-3l$ ADDs were sufficient to detect l largest ADDs, and so $3l$ ADDs are searched around one EQ in the present application. Then, l smaller ADDs among the $3l$ ADDs are discarded at the smallest hypersphere, and only $2l$ ADDs are followed as important reaction routes with expanding hypersphere radii. This ADD following can efficiently be made by a predictor-corrector manner.[35] Although these $2l$ ADDs are followed simultaneously, the ADD following is terminated when l reaction pathways enter into another potential well. This criterion to accept just l routes with closer TSs is also considered

for finding lower energy EQs based on the BEP principle.[51,52] After entering into another potential well, geometry optimizations are made to search for new EQs by using the RFO method.[43] In the present application, $l = 5$ was used.

Although, TSs can be obtained in general applications of the SHS method,[34−36] TSs are discarded in this study, since characterization of EQ−TS−EQ connections by IRC following calculations from all obtained TSs are much demanding on a PES based on reliable quantum chemical calculations.

Acknowledgment. The present work has been financially supported by the Ministry of Education, Science, Sports, and Culture, by its Grants-in-Aid of Scientific Research No.17655001, and a Grant-in-Aid for COE project, Giant Molecules and Complex System, 2004. S. Maeda is supported by Research Fellowship of the Japan Society for Promotion of Science for Young Scientists. Structure refinement calculations on the B3LYP/6-311+G(d,p) surface and energy refinement calculations at the MP2/6-311++G(3df,2p) level have been performed using the parallel computing system in Tohoku University Information Synergy Center. We are grateful for a suggestion by one of reviewers to make comparisons between B3LYP and MP2 frequencies in Section 4E, which has been important to estimate the more reliable T_t value in Section 4A.

Supporting Information Available: A list of geometries in the Cartesian representation for 164 minimum energy structures and an additional C_s cubic structure optimized on the B3LYP/6-311+G(d,p) surface. The list includes relative energy values (potential energy, internal energy, and free energy at 400 K) of each minima at MP2/6-311++G(3df,2p) and B3LYP/6-311+G(d,p) levels and harmonic frequencies by B3LYP/6-311+G(d,p) calculations. This material is available free of charge via the Internet at http://pubs.acs.org.

References and Notes

(1) Kistenmacher, H.; Lie, G. C.; Popkie, H.; Clementi, E. *J. Chem. Phys.* **1974**, *61*, 546.
(2) Stillinger, F. H.; David, C. W. *J. Chem. Phys.* **1980**, *73*, 3384.
(3) David, C. W. *J. Chem. Phys.* **1980**, *73*, 5395.
(4) Brink, G.; Glasser, L. *J. Phys. Chem.* **1984**, *88*, 3412.
(5) Kim, K. S.; Dupuis, M.; Lie, G. C.; Clementi, E. *Chem. Phys. Lett.* **1986**, *131*, 451.
(6) Tsai, C. J.; Jordan, K. D. *J. Chem. Phys.* **1991**, *95*, 3850.
(7) Wales, D. J.; Hodges, M. P. *Chem. Phys. Lett.* **1998**, *286*, 65.
(8) Kabrede, H.; Hentschke, R. *J. Phys. Chem. B* **2003**, *107*, 3914.
(9) James, T.; Wales, D. J.; Hernández-Rojas, J. *Chem. Phys. Lett.* **2005**, *415*, 302.
(10) Buck, U.; Ettischer, I.; Melzer, M.; Buch, V.; Sadlej, J. *Phys. Rev. Lett.* **1998**, *80*, 2578.
(11) Gruenloh, C. J.; Carney, J. R.; Arrington, C. A.; Zwier, T. S.; Fredericks, S. Y.; Jordan, K. D. *Science* **1997**, *276*, 1678.
(12) Gruenloh, C. J.; Carney, J. R.; Hagemeister, F. C.; Arrington, C. A.; Zwier, T. S.; Fredericks, S. Y.; Wood, J. T., III; Jordan, K. D. *J. Chem. Phys.* **1998**, *109*, 6601.
(13) Xantheas, S. S.; Aprà, E. *J. Chem. Phys.* **2004**, *120*, 823.
(14) Wales, D. J.; Ohmine, I. *J. Chem. Phys.* **1993**, *98*, 7257.
(15) Laria, D.; Rodriguez, J.; Dellago, C.; Chandler, D. *J. Phys. Chem. A* **2001**, *105*, 2646.
(16) Tsai, C. J.; Jordan, K. D. *J. Phys. Chem.* **1993**, *98*, 5208.
(17) McDonald, S.; Ojamäe, L.; Singer, S. J. *J. Phys. Chem. A* **1998**, *102*, 2824.
(18) Belair, S. D.; Francisco, J. S. *Phys. Rev. A* **2003**, *67*, 063206.
(19) Blanton, W. B.; Gordon-Wylie, S. W.; Clark, G. R.; Jordan, K. D.; Wood, J. T.; Geiser, U.; Collins, T. J. *J. Am. Chem. Soc.* **1999**, *121*, 3551.
(20) Vegiri, A.; Farantos, S. C. *J. Chem. Phys.* **1993**, *98*, 4059.
(21) Wales, D. J.; Ohmine, I. *J. Chem. Phys.* **1993**, *98*, 7245.
(22) Tsai, C. J.; Jordan, K. D. *J. Chem. Phys.* **1993**, *99*, 6957.
(23) Pedulla, J. M.; Jordan, K. D. *Chem. Phys.* **1998**, *239*, 593.
(24) Rodriguez, J.; Laria, D.; Marceca, E. J.; Estrin, D. A. *J. Chem. Phys.* **1999**, *110*, 9039.
(25) Nigra, P.; Carignano, M. A.; Kais, S. *J. Chem. Phys.* **2001**, *115*, 2621.
(26) Tharrington, A. N.; Jordan, K. D. *J. Phys. Chem. A* **2003**, *107*, 7380.
(27) Kim, J.; Mhin, B. J.; Lee, S. J.; Kim, K. S. *Chem. Phys. Lett.* **1994**, *219*, 243.
(28) Jensen, J. O.; Krishnan, P. N.; Burke, L. A. *Chem. Phys. Lett.* **1995**, *246*, 13.
(29) Smith, A.; Vincent, M. A.; Hillier, I. H. *J. Phys. Chem. A* **1999**, *103*, 1132.
(30) Lee, H. M.; Suh, S. B.; Lee, J. Y.; Tarakeshwar, P.; Kim, K. S. *J. Chem. Phys.* **2000**, *112*, 9759.
(31) Maheshwary, S.; Patel, N.; Sathyamurthy, N.; Kulkarni, A. D.; Gadre, S. R. *J. Phys. Chem. A* **2001**, *105*, 10525.
(32) Miyake, T.; Aida, M. *Chem. Phys. Lett.* **2006**, *427*, 215.
(33) Day, M. B.; Kirschner, K. N.; Shields, G. C. *Int. J. Quantum Chem.* **2005**, *102*, 565.
(34) Ohno, K.; Maeda, S. *Chem. Phys. Lett.* **2004**, *384*, 277.
(35) Maeda, S.; Ohno, K. *J. Phys. Chem. A* **2005**, *109*, 5742.
(36) Ohno, K.; Maeda, S. *J. Phys. Chem. A* **2006**, *110*, 8933.
(37) Fukui, K. *Acc. Chem. Res.* **1981**, *14*, 363.
(38) Page, M.; McIver, J. W., Jr. *J. Chem. Phys.* **1988**, *88*, 922.
(39) Schlegel, H. B. *J. Comput. Chem.* **2003**, *24*, 1514.
(40) Neirotti, J. P.; Calvo, F.; Freeman, D. L.; Doll, J. D. *J. Chem. Phys.* **2000**, *112*, 10340.
(41) Calvo, F.; Neirotti, J. P.; Freeman, D. L.; Doll, J. D. *J. Chem. Phys.* **2000**, *112*, 10350.
(42) Frisch, M. J.; Trucks, G. W.; Schlegel, H. B.; Scuseria, G. E.; Robb, M. A.; Cheeseman, J. R.; Montgomery, Jr., J. A.; Vreven, T.; Kudin, K. N.; Burant, J. C.; Millam, J. M.; Iyengar, S. S.; Tomasi, J.; Barone, V.; Mennucci, B.; Cossi, M.; Scalmani, G.; Rega, N.; Petersson, G. A.; Nakatsuji, H.; Hada, M.; Ehara, M.; Toyota, K.; Fukuda, R.; Hasegawa, J.; Ishida, M.; Nakajima, T.; Honda, Y.; Kitao, O.; Nakai, H.; Klene, M.; Li, X.; Knox, J. E.; Hratchian, H. P.; Cross, J. B.; Adamo, C.; Jaramillo, J.; Gomperts, R.; Stratmann, R. E.; Yazyev, O.; Austin, A. J.; Cammi, R.; Pomelli, C.; Ochterski, J. W.; Ayala, P. Y.; Morokuma, K.; Voth, G. A.; Salvador, P.; Dannenberg, J. J.; Zakrzewski, V. G.; Dapprich, S.; Daniels, A. D.; Strain, M. C.; Farkas, O.; Malick, D. K.; Rabuck, A. D.; Raghavachari, K.; Foresman, J. B.; Ortiz, J. V.; Cui, Q.; Baboul, A. G.; Clifford, S.; Cioslowski, J.; Stefanov, B. B.; Liu, G.; Liashenko, A.; Piskorz, P.; Komaromi, I.; Martin, R. L.; Fox, D. J.; Keith, T.; Al-Laham, M. A.; Peng, C. Y.; Nanayakkara, A.; Challacombe, M.; Gill, P. M. W.; Johnson, B.; Chen, W.; Wong, M. W.; Gonzalez, C.; Pople, J. A. *GAUSSIAN 03, Revision C.02*; Gaussian, Inc.: Wallingford CT, 2004.
(43) Farkas, Ö.; Schlegel, H. B. *J. Chem. Phys.* **1999**, *111*, 10806.
(44) Doye, J. P. K.; Wales, D. J. *J. Chem. Phys.* **1994**, *102*, 9659.
(45) Wales, D. J.; Doye, J. P. K.; Miller, M. A.; Mortenson, P. N.; Walsh, T. R. *Adv. Chem. Phys.* **2000**, *115*, 1.
(46) Jorgensen, W. L.; Chandrasekhar, J.; Madura, J. D.; Impey, R. W.; Klein, M. L. *J. Chem. Phys.* **1983**, *79*, 926.
(47) Jensen, F. *Introduction to Computational Chemistry;* Wiley: Chichester, U.K., 1998.
(48) Jiang, J.-C.; Wang, Y.-S.; Chang, H.-C.; Lin, S. H.; Lee, Y. T.; Niedner-Schatteburg, G.; Chang, H.-C. *J. Am. Chem. Soc.* **2000**, *122*, 1398.
(49) Jiang, J. C.; Chang, H.-C.; Lee, Y. T.; Lin, S. H. *J. Phys. Chem. A* **1999**, *103*, 3123.
(50) Boys, S. F.; Bernardi, F. *Mol. Phys.* **1970**, *19*, 553.
(51) Bell, R. P. *Proc. R. Soc. London, Ser. A* **1936**, *154*, 414.
(52) Evans, M. G.; Polanyi, M. *Trans. Faraday Soc.* **1936**, *32*, 1333.
(53) Goedecker, S. *J. Chem. Phys.* **2004**, *120*, 9911.